An Efficient Antidisturbance Sliding-Mode Speed Control Method for PMSM Drive Systems

Wei Xu, *Senior Member, IEEE*, Abdul Khalique Junejo, Yi Liu, *Senior Member, IEEE*, Mohamed G. Hussien, and Jianguo Zhu, *Senior Member, IEEE*

***Abstract*—A novel sliding-mode-based extended state observer (SMESO) is proposed to improve the disturbance rejection ability and enhance the dynamic performance of permanent magnet synchronous motor drive systems. First, an extended state observer based on the fast terminal sliding-mode control (FTSMC) method is developed for better comparison, which can improve the robustness against load disturbances, finite time convergence, and get effective reduction of the chattering phenomenon. The SMESO-based FTSMC is then developed by using the SMESO to estimate the system total disturbance, and input the signal to a feed-forward compensation controller to further improve the system dynamic performance. The closed-loop stability analysis is conducted by using the Lyapunov stability function. The superior effectiveness of the proposed method is confirmed by comprehensive simulation and experiments.**

***Index Terms*—Conventional sliding-mode control, fast terminal sliding mode control (FTSMC), Lyapunov stability function, permanent magnet synchronous motor (PMSM), sliding-mode-based extended state observer (SMESO).**

I. Introduction

THE permanent magnet synchronous motor (PMSM) has many advantages, such as high power density and high efficiency, and thus is widely used in various high-performance applications, such as electric vehicles (EVs), robotic systems, computer numerical control (CNC) machines, and so on [1]. To achieve excellent drive performance in modern applications, the motor drive system needs to be carefully designed [2]. The linear control algorithms, e.g., the proportional integral (PI), are commonly used in the PMSM speed control due to their simplicity in design and implementation [3]. However, the PMSM drive system is nonlinear and multivariable with various internal disturbances (parametric change and unmodeled dynamics) and external disturbances (load torque change) [4]. While the internal disturbances can be suppressed by the closed loop control, the external disturbances would unavoidably cause fluctuations in the PMSM speed response, deteriorating the control performance of the PI speed controller. These speed fluctuations cannot be ignored in many high-performance applications, such as EVs and CNC machines.

Various nonlinear algorithms have been developed to improve the disturbance rejection ability of speed controllers, including adaptive control [3], [4], robust control [5], [6], fuzzy control [7], disturbance observer (DO) control [8], sliding-mode control (SMC) [9], etc. Among these algorithms, the DO-based control method is a better choice to improve the disturbance rejection ability of the drive systems. In 1987, Ohnishi developed the first DO to improve the disturbance rejection ability [10]. This method is then used in many industrial applications [8], [10]. Due to the simple structure, the DO-based control method is widely employed in many control applications, but its dynamic control performance and load disturbance rejection ability are very limited. To address these problems, various nonlinear DO-based control methods are developed [11], [12]. In [11], the nonlinear DO-based controller is proposed to estimate the disturbances in robotic control systems, and in [12], the neural-network-based nonlinear DO is employed to estimate the disturbances in motor control systems. The DO-based control algorithms have been paid more and more attentions for the speed control of PMSM drive systems. In general, the estimation of load disturbances is the main issue in the DO-based speed control systems.

In [13] and [14], an extended state observer (ESO) is developed for the PMSM drive, and the load torque is taken as the extended state variable. However, under the load disturbances, the performance of PMSM drive systems with the linear ESO is limited. The nonlinear ESO-based SMC has been designed for the PMSM speed control against the load disturbances, but the chattering phenomenon in the control input of the system is generated due to the inherent high switching frequency of the SMC. Zhang *et al.* [15] introduced an ESO-based SMC to

Manuscript received May 31, 2020; revised August 31, 2020; accepted November 16, 2020. Date of publication November 23, 2020; date of current version February 5, 2021. This work was supported in part by the National Natural Science Foundation of China under Grants 51877093 and 51707079, in part by the National Key Research and Development Program of China under Grant 2018YFE0100200, and in part by the Key Technical Innovation Program of Hubei Province under Grant 2019AAA026. Recommended for publication by Associate Editor J. Zhang. (*Corresponding author: Abdul Khalique Junejo*.)

Wei Xu, Yi Liu, and Mohamed G. Hussien are with the State Key Laboratory of Advanced Electromagnetic Engineering and Technology, School of Electrical and Electronic Engineering, Huazhong University of Science and Technology, Wuhan 430074, China (e-mail: weixu@hust.edu.cn; liuyi82@hust.edu.cn; mohamed.hussien3@f-eng.tanta.edu.eg).

Abdul Khalique Junejo is with the State Key Laboratory of Advanced Electromagnetic Engineering and Technology, School of Electrical and Electronic Engineering, Huazhong University of Science and Technology, Wuhan 430074, China, and also with the Department of Electrical Engineering, Qaid-e-Awam University of Engineering, Science and Technology, Nawabshah 67450, Pakistan (e-mail: ak.junejo@gmail.com).

Jianguo Zhu is with the School of Electrical and Information Engineering, University of Sydney, Sydney, NSW 2006, Australia (e-mail: jianguo.zhu@sydney.edu.au).

Color versions of one or more of the figures in this article are available at https://doi.org/10.1109/TPEL.2020.3039474.

Digital Object Identifier 10.1109/TPEL.2020.3039474

estimate the load torque, but the chattering phenomenon still exists in the designed ESO. The first- and second-order observers are also developed to estimate the disturbances, but the dynamic performance of these observers is relatively poor against the load disturbances [6], [8]. The antidisturbance ability and speed fluctuations of the PMSM drive system can be further improved to design advanced nonlinear speed control methods.

Therefore, the sliding-mode-based extended state observer (SMESO) is proposed to combine with the corresponding sliding mode surface as fast terminal sliding mode control (FTSMC) method to further improve the disturbance rejection ability and reduce the speed fluctuations of the PMSM speed control system. The SMESO is regarded as an observer, which is used to estimate the system total disturbance, and the observed signal is fed to a feed-forward compensation controller to further improve the system dynamic performance by enhancing the load disturbance rejection ability of the PMSM speed control system. The proposed method can improve not only the disturbance rejection ability, but also the starting and load transient time, steady-state dynamics, and minimization of the chattering phenomenon of the system effectively. In this article, the FTSMC is selected as sliding-mode surface since its performance is superior to those of the conventional SMC (CSMC) and terminal SMC (TSMC) [16] and [17].

The rest of article is organized as follows. Section II presents the mathematical model of the PMSM and SMC design algorithm with numerical simulations to show the superiority of FTSMC than the conventional sliding mode surfaces. In Section III, the FTSMC is fully designed for the PMSM speed control. In Section IV, an antidisturbance SMESO is put forward to the estimation of total disturbances in the drive system. Comprehensive simulation and experiments in Section V have fully demonstrated that the PMSM drive system based on the proposed algorithm can enjoy the efficient antidisturbance ability for the speed regulation. Finally, the conclusion are made in Section VI.

II. System Modeling

This section presents the mathematical model of the PMSM drive system and the second-order nonlinear system is chosen to validate the superiority of the FTSMC over the CSMC and TSMC, respectively.

A. PMSM Mathematical Model

The mathematical model of the PMSM in the synchronous rotating *dq*-frame can be expressed as

$$\dot{\omega} = \frac{M_t}{J} i_q - \frac{B}{J}\omega - \frac{n_p}{J} T_L \tag{1}$$

$$\dot{i}_d = -\frac{R_s}{L_s} i_d + n_p \omega i_q + \frac{u_d}{L_s} \tag{2}$$

$$\dot{i}_q = -\frac{R_s}{L_s} i_q + n_p \omega i_d - \frac{n_p \omega \psi_f}{L_s} + \frac{u_q}{L_s} \tag{3}$$

where ω is the PMSM electrical speed, $M_t = 2/3\ {n_p}^2 \psi_f$, $m = M_t/J$, n_p the number of pole pairs, ψ_f the magnetic flux linkage, J the coefficient of inertia the moment of inertia, B the viscous damping coefficient, T_L the load torque, and u_d, u_q, i_d, and i_q are the d- and q-axis voltages and currents, respectively. R_s and L_s the resistance and the synchronous inductance of the stator, respectively. Fig. 1 shows a block diagram of the general field orientation control (FOC) of the PMSM, containing two control loops for the current and speed, respectively. When $i_d = 0$, the PMSM is operating in the constant torque mode. Two PI controllers are employed in the current loop to regulate the current dynamics simultaneously.

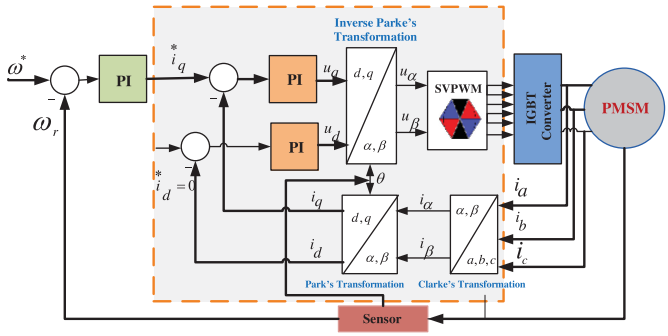

Fig. 1. Structure diagram of the PMSM drive under the FOC method.

B. SMC Design Procedure

Compared to other nonlinear control methods, the SMC is more insensitive to the internal and external disturbances, since when the system state reaches the sliding surface, it will stay on the designed sliding surface. The SMC can be put forward in two steps: 1) the sliding surface design, and 2) the reaching law design, which forces the system state to reach and stay on the designed sliding surface. The reaching condition of SMC can be expressed as

$$s\dot{s} < 0 \tag{4}$$

where s is the sliding trajectory.

As an example to describe the SMC design procedure, a second-order system is used as

$$\begin{cases} \dot{\vartheta}_1 = \vartheta_2 \\ \dot{\vartheta}_2 = r(\vartheta) + w(\vartheta) + q(\vartheta)u \end{cases} \tag{5}$$

where $\vartheta = [\vartheta_1, \vartheta_2]^T$ is the system state,$w(\vartheta)$ the total disturbances, $q(\vartheta) \neq 0$, and u the system control input. The FTSMC has superior performance than the conventional sliding mode surfaces (such as CSMC and TSMC), which is chosen as the sliding surface [16], as illustrated by

$$s = \vartheta_2 + \sigma_1 |\vartheta_2|^{\alpha_1} \mathrm{sign}(\vartheta_2) + \sigma_2 |\vartheta_1|^{\alpha_2} \mathrm{sign}(\vartheta_1) \tag{6}$$

where $\sigma_1 > 0$,$\sigma_2 > 0$, $0 < \alpha_1 < 2$, $\alpha_2 > \alpha_1$, and $\alpha_1 = p/q$, both p and q are odd positive numbers.

The reaching law is designed in such a way that the system state must reach the designed sliding surface, and satisfy the aforementioned reaching condition. To meet the requirements, the terminal sliding mode reaching law (TSMRL) is chosen, which has advantages of fast convergence, robust steady-state dynamics, and smaller chattering than the constant rate reaching

law and exponential reaching law [16], respectively, as expressed by

$$\dot{s} = -k_1 s - k_2 |s|^{\alpha_3} \text{sign}(s) \tag{7}$$

where k_1 and k_2 are the coefficients of the reaching law, and $0 < \alpha_3 < 1$. Taking derivative of (6), and then combining with (7) yields

$$-k_1(s) - k_2|s|^{\alpha_3}\text{sign}(\vartheta) = \dot{\vartheta}_2 + \alpha_1\sigma_1|\vartheta_2|^{\alpha_1-1}\dot{\vartheta}_2\text{sign}(\vartheta_2) + \alpha_2\sigma_2|\vartheta_1|^{\alpha_2-1}\dot{\vartheta}_1\text{sign}(\vartheta_1). \tag{8}$$

Next, by combining (5) and (8), the control input u can be obtained as

$$u = -\frac{1}{q(\vartheta)}[r(\vartheta) + w(\vartheta) + \alpha_1\sigma_1|\vartheta_2|^{\alpha_1-1}\text{sign}(\vartheta_2) + \alpha_2\sigma_2|\vartheta_1|^{\alpha_2-1}\dot{\vartheta}_1\text{sign}(\vartheta_1) + k_1(s) + k_2|s|^{\alpha_3}\text{sign}(\vartheta)]. \tag{9}$$

In (9), two discontinuous terms of $1/q(\vartheta)$ and $k_2|\vartheta|^{\alpha_3}\text{sign}(\vartheta)$ could cause the chattering phenomenon in the system. The chattering level of the designed SMC control law is proportional to the switching gain value of the designed reaching law (k_1 and k_2). The larger value of the k_1 and k_2 would cause a larger chattering phenomenon in the system, and vice versa. It is noted that when the switching gain value of the SMC control law is selected as smaller, the antidisturbance ability of the control system can be compromised to some extent. Therefore, it is very important to make optimization on the switching gain for the proposed control law.

C. Comparison of the FTSMC, Conventional SMC, and TSMC

The sliding surfaces of the CSMC [17] and TSMC [18] can be expressed as

$$s = \vartheta_2 + c\vartheta_1 \tag{10}$$

$$s = \vartheta_1 + \frac{1}{\beta}\vartheta_2^{p/q} \tag{11}$$

where c and β are positive coefficients, and p and q are two odd constants.

Through numerical analysis of different sliding surfaces, the control performances of the linear SMC, TSMC, and FTSMC are fully compared. Main parameters are selected as $r = -25\dot{\vartheta}_1$, $q = 133$, $\rho = 10\sin(\pi t)$, and $x_a = \sin(t)$ (the ideal position signal). The initial state of the controlled object $\vartheta(0)$ is set as $[\vartheta_1, \vartheta 2] = [-1000, -1000]$.

Fig. 2 compares the performance of the CSMC, TSMC, and FTSMC. As shown in this figure, the FTSMC is evidently superior to the CSMC and TSMC for its fastest convergence and tracking response to the reference value. Due to the aforementioned stunning properties, the FTSMC is selected as the sliding trajectory.

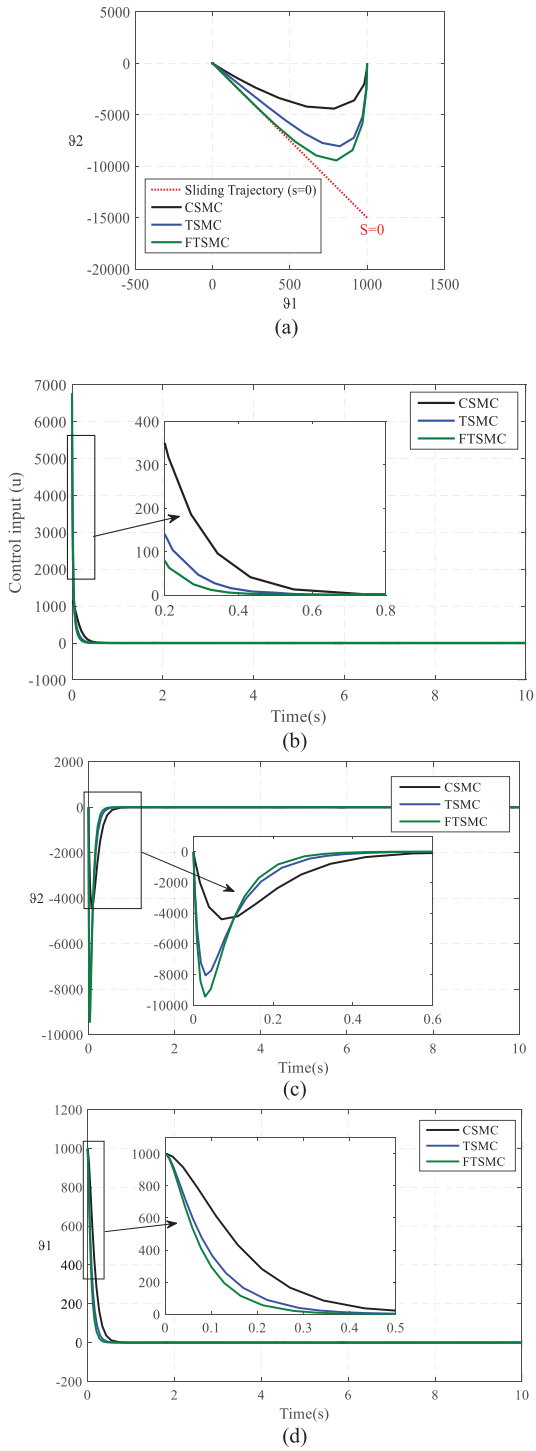

Fig. 2. Comparison of control performances of the CSMC, TSMC, and FTSMC for one PMSM drive system. (a) Phase trajectory of the sliding surface. (b) Control input response. (c) Derivative of the error response. (d) Error response of the system.

III. Controller Design

The speed controller is adopted to suppress the total disturbances of the system. The governing equation of the speed of PMSM system under total disturbances can be expressed as

$$\dot{\omega} = \frac{M_t}{J}i_q^* - \frac{B}{J}\omega + D(t) \tag{12}$$

where $D(t)$ is the total disturbance, as calculated by

$$D(t) = -\frac{B}{J}\omega - \frac{n_p T_L}{J} - \frac{M_t}{J}(i_q^* - i_q). \tag{13}$$

A. Speed Controller Design Based on the FTSMC

The speed error of the PMSM system can be written as

$$\varepsilon = \omega^* - \omega \tag{14}$$

where $\omega^*$and ω are the reference and actual speeds of the PMSM, respectively. Taking derivatives of (14) and then substituting into (12), it will get

$$\dot{\varepsilon} = \dot{\omega}^* - \frac{M_t}{J} i_q^* - D(t). \tag{15}$$

The sliding surface is needed to design the SMC-based speed controller of the PMSM drive system. As discussed previously, the FTSMC expressed by (6) is preferred as the sliding mode surface because of its superior capability than those of the TSMC and CSMC, respectively. Another part of SMC is the reaching phase, in which one suitable reaching law should be designed to satisfy $s\dot{s} < 0$. In this article, the FTSMC (6) with TSMRL (7) is chosen as the sliding mode surface and reaching law, respectively.

The speed error (14) is chosen as the system state variable, which should reach to zero or $s = 0$ .Meanwhile, the FTSMC sliding surface is decided by (6) and the TSMRL reaching law based on (7). Hence, the FTSMC-based speed controller can be described as

$$i_q^* = m^{-1}[\mu_{\text{eq}} + \mu_b + D(t)] \tag{16}$$

$$\mu_{\text{eq}} = \dot{\omega}^* + \sigma_1|\dot{\varepsilon}|^{\alpha_1}\text{sign}(\dot{\varepsilon}) + \sigma_2|\varepsilon|^{\alpha_2}\text{sign}(\varepsilon) \tag{17}$$

$$\mu_b = \int_0^t k_1(s) + k_2|s|^{\alpha_3}\text{sign}(s)dt. \tag{18}$$

Then, the Lyapunov function is used to verify the system stability. According to (6), the FTSMC can be expressed as

$$\begin{aligned} s &= \dot{\varepsilon} + \sigma_1|\dot{\varepsilon}|^{\alpha_1}\text{sign}(\dot{\varepsilon}) + \sigma_2|\varepsilon|^{\alpha_2}\text{sign}(\varepsilon) \\ &= \dot{\omega}^* - mi_q^* - D(t) + \sigma_1|\dot{\varepsilon}|^{\alpha_1}\text{sign}(\dot{\varepsilon}) \\ &\quad + \sigma_2|\varepsilon|^{\alpha_2}\text{sign}(\varepsilon). \end{aligned} \tag{19}$$

Substituting (16)–(18) into (19), the sliding surface can be described as

$$\begin{aligned} s = \dot{\omega}^* - m[m^{-1}(\mu_{\text{eq}} + \mu_b)] - D(t) + \sigma_1|\dot{\varepsilon}|^{\alpha_1}\text{sign}(\dot{\varepsilon}) \\ + \sigma_2|\varepsilon|^{\alpha_2}\text{sign}(\varepsilon). \end{aligned} \tag{20}$$

Meanwhile, (20) can be simplified as

$$s = -\mu_b - D(t). \tag{21}$$

Taking derivative of (21) and then substituting the TSMRL (7) into (21) yields

$$\dot{s} = -\dot{\mu}_b - \dot{D}(t) = -k_1(s) - k_2|s|^{\alpha_3}\text{sign}(s) - \dot{D}(t) \tag{22}$$

or

$$\dot{s}s = [-k_1(s) - k_2|s|^{\alpha_3}\text{sign}(s) - \dot{D}(t)]s. \tag{23}$$

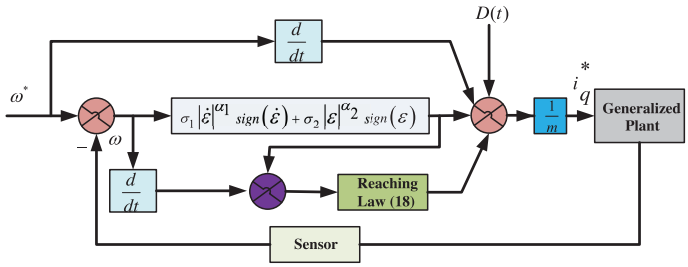

Fig. 3. Block diagram of the FTSMC for the speed regulation.

According to the Lyapunov function ($V = ½\, s^2$), (23) can be expressed as

$$\begin{aligned} \dot{V} = \dot{s}s &= [-k_1(s) - k_2|s|^{\alpha_3}\text{sign}(s) - \dot{D}(t)]s \\ &\le -k_1(s)^2 - k_2|s|^{\alpha_3+1} + \left|\dot{D}(t)\right||s| \\ &\le -k_1(s)^2 - \left[k_2 - \frac{\left|\dot{D}(t)\right|}{|s|^{\alpha_3}}\right]|s|^{\alpha_3+1} \\ &\le -k_1(s)^2 - [k_2 - \zeta_D]\,|s|^{\alpha_3+1} \\ &= -2\Omega_1 V - 2^{\frac{\alpha_3+1}{2}}\Omega_2 V^{\frac{\alpha_3+1}{2}} \end{aligned} \tag{24}$$

where Ω_1 and Ω_2 are the positive constants. Equation (24) confirms that, if $k_2 > \zeta_D$, the speed error must converge to zero within the finite time, as illustrated by

$$\begin{aligned} t_{sf} = \int_0^{\varepsilon(0)} \frac{{\sigma_1}^{1/\alpha_1}}{\left(\varepsilon + \sigma_2\varepsilon^{\alpha_2}\right)^{1/\alpha_2}} d\varepsilon = \frac{\sigma_1|\varepsilon(0)|^{1-1/\alpha_1}}{\sigma_2(\sigma_1 - 1)} \\ \cdot R\left(\frac{1}{\alpha_1}; \frac{\alpha_1 - 1}{(\alpha_2 - 1)\alpha_1}; 1 + \frac{\alpha_1 - 1}{(\alpha_2 - 1)\alpha_1}; -\sigma_2|\varepsilon(0)|^{\alpha_2 - 1}\right) \end{aligned} \tag{25}$$

where $R(\cdot)$ shows the Gauss hypergeometric (GH) function and the conditions α_1, α_2, and k_2 induce that $R(\cdot)$ must remain convergent. The detailed derivation of (25) and GH function can be founded in [19]. Meanwhile, (25) shows that the system state can arrive at the sliding mode surface in the definite time, i.e., converging to zero in the finite time.

Fig. 3 shows that the design procedure of the generated reference i_q^* based on the FTSMC, which is relatively simple and easy to be realized by the DSP software. It can be seen from (16) and Fig. 3, which have the disturbance $D(t)$ term. The disturbance $D(t)$ has great influence on the control performance of the PMSM, which cannot be measured directly. It should note that (7) has the k_1 and k_2 switching gains, which are directly proportional to the $D(t)$. In general, the higher values of the switching gains can produce the chattering of the system. Hence, the minimum values of (7) should be selected to increase the robustness of the drive system. Therefore, in order to estimate the disturbances and then make effective compensation, one improved antidisturbance SMESO is proposed in this article. It can successfully reduce the chattering phenomenon and strengthen

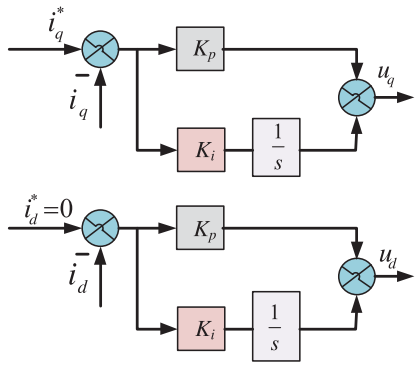

Fig. 4. Simple diagram of PI current controllers.

the antidisturbance ability of the close-loop control on the whole drive system.

B. Current Controller

In order to get good balance between the tracking precision and computing burden, the PI controllers are employed for the current controllers for the PMSM drive system. In general, the mathematical expression of *dq*-axis voltage, u_d, can be written as

$$u_{dq} = K_P e_{dq} + \int K_i e_{dq} \tag{26}$$

where k_p and k_i are PI gains, and e_{dq} is the error of *dq*-axis currents between reference and actual values and can be calculated by

$$e_{dq} = i_{dq}^* - i_{dq} \tag{27}$$

where i_{dq}^* and i_{dq} are the reference and actual *dq*-axis currents, respectively. The block diagram of PI current controllers is shown in Fig. 4.

IV. Design of Antidisturbance SMESO

A. Conventional ESO

A first-order system in this article can be expressed as

$$\begin{aligned} z_1(t) &= h(z_1) + gu(t) \\ y(t) &= z_1(t) \end{aligned} \tag{28}$$

where $h(z_1)$ is the perturbation function, g a constant gain, and $u(t)$ the control input of the system. By choosing $z_2(t)$, as defined by $\dot{z}_2(t) = Q(t)$, the system (28) can be expanded as

$$\begin{aligned} \dot{z}_1(t) &= z_2(t) + gu(t) \\ \dot{z}_2(t) &= Q(t) \\ y(t) &= z_1(t). \end{aligned} \tag{29}$$

Assuming $u(t) = i_q^*$ and $z_1(t) = \omega$ in (29), one can obtain the conventional ESO by combining (12), (28), and (29), as described by

$$\begin{aligned} \varepsilon_1(t) &= v_2(t) - \omega \\ \dot{v}_1(t) &= v_2(t) + mi_q - \eta_1\varepsilon_1(t) \\ \dot{v}_2(t) &= -\eta_2\varepsilon_1(t) \end{aligned} \tag{30}$$

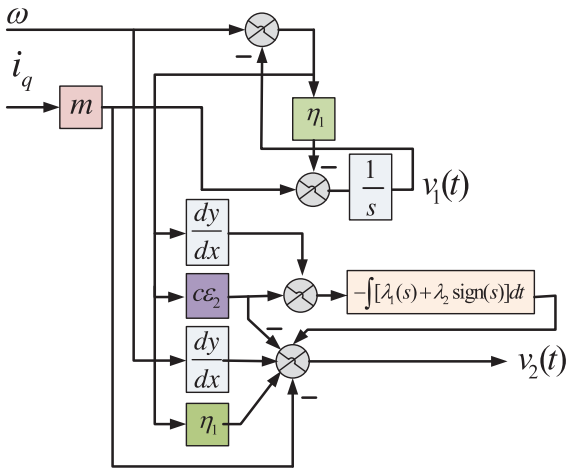

Fig. 5. Diagram of the SMESO based FTSMC method for the speed loop.

where η_1 and η_2 are two positive constant coefficients. The feedback speed and total disturbance signals of the PMSM can be obtained by $v_1(t)$ and $v_2(t)$, respectively. Then, the feed-forward compensation can be achieved.

B. Design of the Speed Controller of Antidisturbance SMESO

In order to improve the speed regulation performance of the PMSM drive system under load disturbances, the SMESO is designed in this section as illustrated in Fig. 5. As seen from this figure, the SMESO can first estimate the disturbances of the PMSM, $v_2(t)$, and then input it to the feed-forward compensation with $i_q{}^*$. In general, the SMESO is designed from (30), and its error can be written as

$$\varepsilon_2(t) = v_1(t) - \omega \tag{31}$$

where $v_1(t)$ and ω are the estimated and actual speeds of the observer, respectively. The sliding mode surface is chosen for the SMESO as expressed by

$$s = \dot{\varepsilon}_2 + c\varepsilon_2. \tag{32}$$

Taking the derivative of (31) and substituting into (32), it can get

$$\dot{s} = \dot{v}_1(t) - \dot{\omega} + c\varepsilon_2. \tag{33}$$

The SMC design needs the reaching law as chosen by

$$\dot{s} = -\lambda_1 s - \lambda_2 \mathrm{sign}(s) \tag{34}$$

where λ_1 and λ_2 are two positive constants. Substituting (33) into (34) yields

$$\int [-\lambda_1(s) - \lambda_2\mathrm{sign}(s)]dt = \dot{v}_1(t) - \dot{\omega} + c\varepsilon_2$$

$$\int [-\lambda_1(s) - \lambda_2\mathrm{sign}(s)]dt = v_2(t) + mi^*q - \eta_1\varepsilon_1(t) - \dot{\omega} + c\varepsilon_2$$

$$\begin{aligned} v_2(t) = &-mi_q + \eta_1\varepsilon_1(t) + \dot{\omega} - c\varepsilon_2 \\ &+ \int [-\lambda_1(s) - \lambda_2\mathrm{sign}(s)]dt. \end{aligned} \tag{35}$$

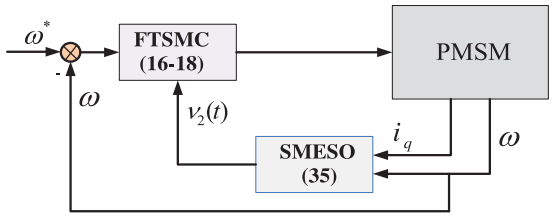

Fig. 6. Block diagram of the proposed (SMESO + FTSMC) method for the speed loop.

The estimated system disturbance is compensated by feeding the output of SMC-based speed controller to the feed-forward compensation. Thereof, the final SMESO-based FTSMC can be rewritten as

$$i_q^* = m^{-1}(\mu_{eq} + \mu_b + v_2(t)). \tag{36}$$

Fig. 6 shows the final antidisturbance speed controller of the PMSM drive system. As seen from this figure, i_q^* is generated through the FTSMC, which is designed based on (16)–(18). The total disturbance can be estimated by the SMESO in terms of (35), and the estimated disturbance is compensated through the feed-forward compensation method.

C. Stability Analysis of the SMESO

To check the stability of SMESO, one selected Lyapunov function can be expressed as

$$\lim_{s\to 0} \dot{V} = \lim_{s\to 0} s\dot{s} \le 0 \tag{37}$$

and

$$\begin{aligned} \dot{V} = s\dot{s} &= s\left[c\varepsilon_2 + \dot{\varepsilon}_2\right] \\ &= s\left[c\varepsilon_2 + \dot{v}_1(t) - \dot{\omega}\right] \\ &= s\left[c\varepsilon_2 + v_2(t) + mi_q^* - \eta_1\varepsilon_1(t) - \dot{\omega}\right] \\ &= s\left[\int\left[-\lambda_1(s) - \lambda_2 \text{sign}(s)\right]dt\right] \\ &= -\lambda_1|s|^2 - \lambda_2|s| \le 0 \end{aligned} \tag{38}$$

where the coefficients λ_1 and λ_2 are positive constant gains, and the negative sign of (38) can ensure the close loop stability of the designed SMESO.

D. Estimated Disturbances of the SMESO

The simulation and experimental responses of the ESO and SMESO from no load to load conditions are shown in Figs. 7 and 8, respectively. It can be seen from Figs. 7 and 8 that the SMESO can estimate the disturbance as ESO, but the estimated disturbance under the SMESO is much quicker than the ESO, respectively. First, the speed controller based on the FTSMC is constructed according to (16), which is used to drive the PMSM. Second, the SMESO can be also designed by using (31), and then the effectiveness of the SMESO can be tested by adding or removing the load suddenly.

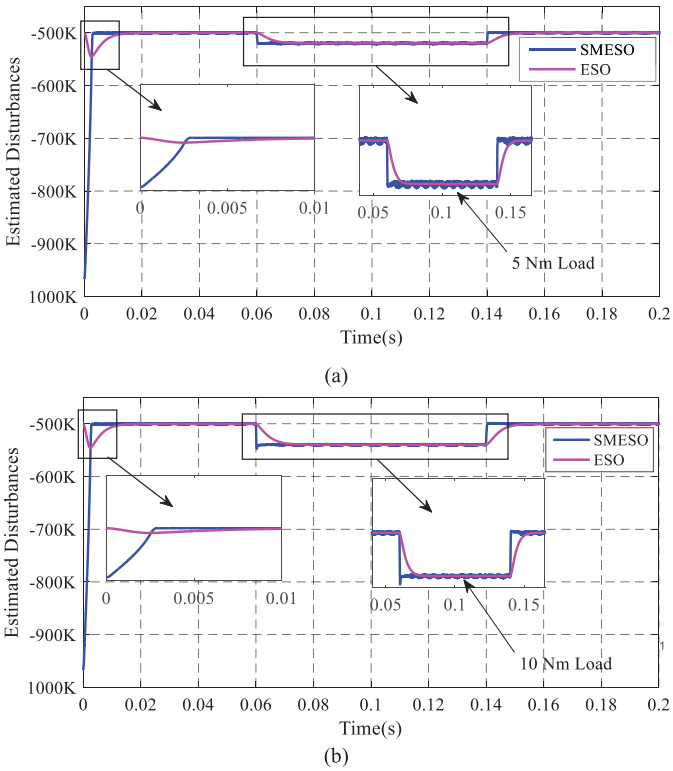

Fig. 7. The estimated disturbances of the ESO and SMESO under load by simulation. (a) 5 Nm load. (b) 10 Nm load.

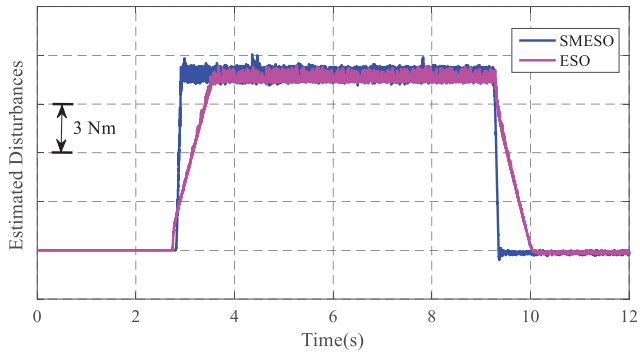

Fig. 8. The estimated disturbances of the ESO and SMESO under 10 Nm load by experiment.

Finally, the estimated disturbances of drive system by the help of SMESO can be considered as the feed-forward part of the speed controller based on the FTSMC. The estimated disturbances under the SMESO has little chattering, as regarded as one inherent property of the SMC, which can be reduced by adopting optimal reaching law.

V. Simulation and Experimental Verification

In order to demonstrate the effectiveness of the proposed method, extensive numerical, dynamic simulation, and experiments have been carried out and fully compared with each other. The speed and q-axis current dynamic performance of the PMSM under the PI, FTSMC, FTSMC + ESO, and FTSMC +

TABLE I
MAIN PARAMETERS OF THE PMSM

Symbol	Name	Value and Unit
n_p	Pole pairs	3
p	Rated power	3.0 kW
n	Rated speed	2000 rpm
R_s	Stator resistance	0.8 Ω
ψ_f	Flux linkage	0.35 Wb
L_s	dq-axis inductances	0.005 H
J	Coefficient ofinertia	$3.78\times10^{-4}\,kg.m^2$
B	Viscous damping coefficient	$1.74\times10^{-5}\,\mathrm{N}\cdot m\cdot s$ / rad

SMESO methods are studied carefully based on three typical working states, including no-load, variable load, and speed reversal conditions. Main parameters of the PMSM are listed in Table I.

A. Simulation and Analysis

The simulation results are compared under no-load, load, and speed reversal conditions by the control of PI, FTSMC, ESO + FTSMC, and SMESO + FTSMC methods. The reference speeds of the speed controller are set as 1000 and 1500 rpm, and the load disturbances as 5 and 10 Nm on PMSM, respectively. More details will be given out as follows.

1) Case-1. Startup and Steady-State Performance: The starting speed responses of the PMSM under the control of PI, FTSMC, ESO + FTSMC, and SMESO + FTSMC methods at no-load are compared. Fig. 9 depicts the dynamic speed and q-axis current responses at no-load. As shown from Fig. 9(a), at starting under no-load, the speed response of the PI controller contains an overshoot, while those of FTSMC, ESO + FTSMC, and SMESO + FTSMC control methods do not. The settling time of the speed responses during the starting process is 0.03870, 0.00297, 0.00285, and 0.00265 s under the control of PI, FTSMC, ESO + FTSMC, and SMESO + FTSMC methods, respectively. It can be seen that the proposed method has faster dynamic response than those of the PI, FTSMC, and ESO + FTSMC, respectively. Moreover, it can be also known that the proposed SMESO + FTSMC has smaller steady-state error than PI, FTSMC, and ESO + FTSMC separately. The q-axis current responses at no-load condition under the PI, FTSMC, ESO + FTSMC, and SMESO + FTSMC methods during the starting process and steady state are shown in Fig. 9(b). As seen from this picture, the proposed SMESO + FTSMC has much quicker response, smaller ripple, and chattering in the q-axis current in comparison to those of the PI, FTSMC, and ESO + FTSMC methods, respectively.

2) Case-2. Steady-State Performance at Different Loads: The speed responses of the PMSM drive system with loads of 5 and 10 Nm under the control of PI, FTSMC, ESO + FTSMC, and SMESO + FTSMC methods are simulated and compared with each other. The speed and q-axis current responses are also simulated with the reference speeds of 1000 and 1500 rpm, respectively.

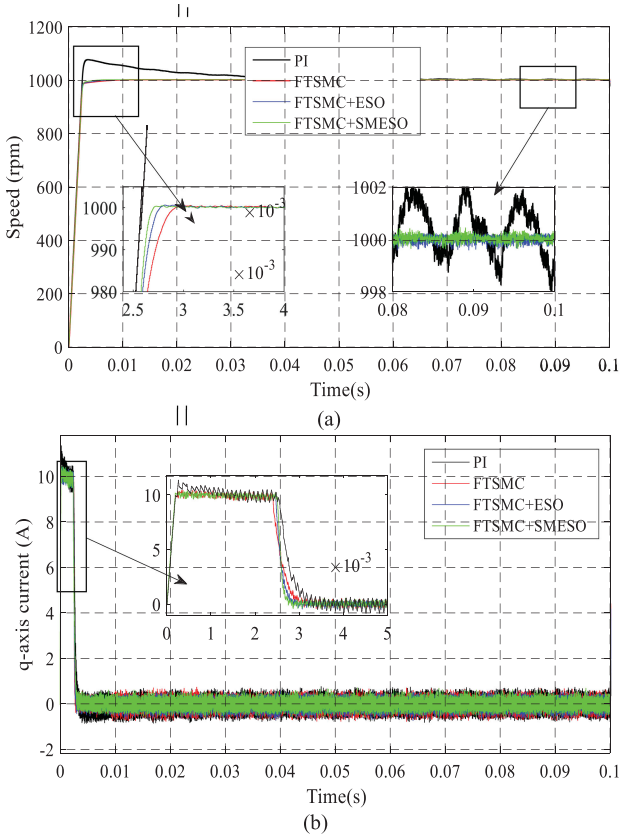

Fig. 9. Startup and steady-state responses of PI, FTSMC, FTSMC + ESO, and SMESO + FTSMC methods under no-load at 1000 rpm. (a) Speed. (b) q-axis current.

It is obvious from Fig. 10(a) that the settling times of the speed responses are 0.034 s under the PI control, 0.023 s under the FTSMC, 0.011 s under the ESO + FTSMC, and 0.010 s under the SMESO + FTSMC. Also, it can be seen that the speed drop under the control of PI, FTSMC, ESO + FTSMC, and SMESO + FTSMC methods is 30, 17, 12, and 9 rpm, respectively.

It can be concluded from above analysis that the SMESO has robust antidisturbances property than the PI, FTSMC, and ESO + FTSMC, separately. Moreover, the q-axis current responses under the PI control, FTSMC, ESO + FTSMC, and SMESO + FTSMC methods at a reference speed of 1000 rpm with load of 5 Nm are shown in Fig. 10(b). As seen from this picture, the SMESO + FTSMC method has fastest transient response, smallest ripple, and chattering in the q-axis current.

When the PMSM is loaded under the PI, FTSMC, ESO + FTSMC, and SMESO + FTSMC methods, the settling time of speed response is 0.35, 0.024, 0.011, and 0.010 s, respectively, as illustrated in Fig. 11(a). As depicted in this figure, the drops of speed response under the PI, FTSMC, ESO + FTSMC, and SMESO + FTSMC are 60, 54, 52, and 47 rpm, respectively. It is seen that the speed fluctuation under the SMESO + FTSMC method is the smallest. Meanwhile, the q-axis current responses under the control of PI, FTSMC, ESO + FTSMC, and the proposed SMESO + FTSMC methods at a reference 1500 rpm with a load of 10 Nm are shown in Fig. 11(b). As seen from

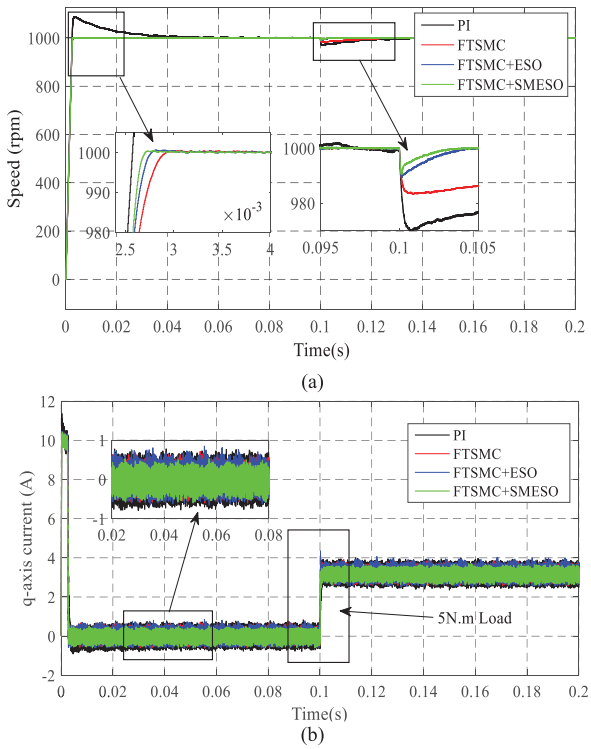

Fig. 10. Sudden load adding responses of PI, FTSMC, FTSMC + ESO, and SMESO + FTSMC methods under 5 Nm at 1000 rpm. (a) Speed. (b) q-axis current.

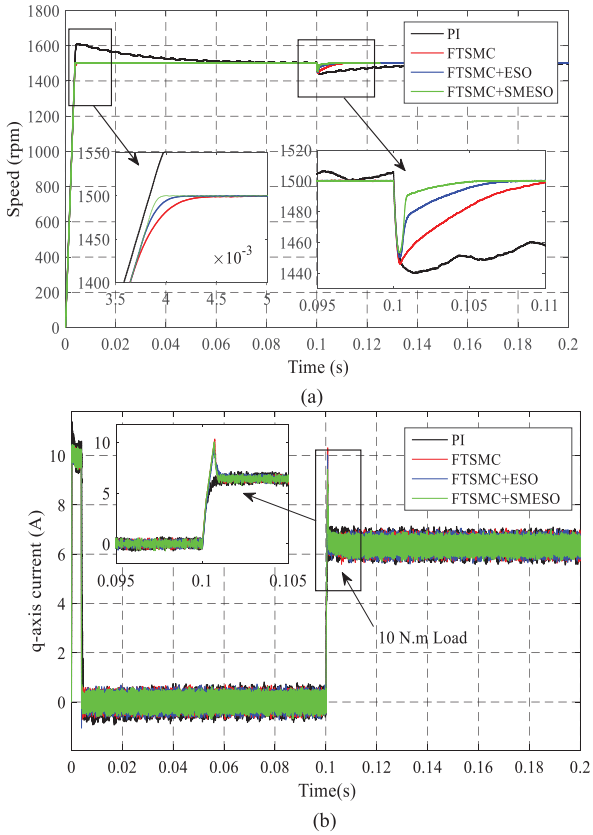

Fig. 11. Sudden load adding responses of PI, FTSMC, FTSMC + ESO, and SMESO + FTSMC methods under 10 Nm at 1500 rpm. (a) Speed. (b) q-axis current.

TABLE II
PERFORMANCE INDEXES DURING STARTUP AND LOAD TRANSIENT BASED ON THE PI, FTSMC, FTSMC + ESO, AND FTSMC + SMESO METHODS

Control Method	Startup Settling Time (s)	Speed Drop (rpm) and Settling Time (s) with 5 NmLoad		Speed Drop (rpm) and Settling Time (s) with 10 Nm Load	
PI	0.03870	30	0.034	60	0.035
FTSMC	0.00297	17	0.023	54	0.024
FTSMC+ESO	0.00285	12	0.011	52	0.011
FTSMC+SMESO	0.00265	9	0.010	47	0.10

this picture, the q-axis current response under the SMESO + FTSMC method has the smallest current ripple, chattering, and shortest settling time.

Some key performance indexes based on the PI, FTSMC, FTSMC + ESO, and FTSMC + SMESO methods are summarized in Table II. It is concluded from Table II that the proposed method, SMESO + FTSMC, has superior performance than those of the PI, FTSMC, and FTSMC + ESO in terms of transient response at starting and rated loading points. Moreover, it is also seen that the proposed method, SMESO + FTSMC, has faster robust antidisturbances response against different load disturbances.

3) Case-3. Speed Reversal and Steady-State Performance: The speed reversal responses and steady-state performance under the control of PI, FTSMC, ESO + FTSMC, and SMESO + FTSMC methods are also compared in details. Fig. 12 shows the speed and q-axis current responses under the control of PI, FTSMC, ESO + FTSMC, and SMESO + FTSMC methods during the speed reversal from 1000 to −1000 rpm, and then −1000 to 1000 rpm. As shown from this figure, the speed response under the PI control has an overshoot while those of FTSMC, ESO + FTSMC, and SMESO + FTSMC methods do not have during the process of speed reversal.

Specifically, Fig. 12(a) also shows that the speed convergence and error tracking precision of the SMESO + FTSMC method are the best among all these control methods during the steady-state and speed reversal operation. Furthermore, as shown in Fig. 12(b), the SMESO + FTSMC method can also get the faster transient response, smaller current ripple, and chattering in the q-axis current.

As demonstrated by the above simulation results, it is known that the SMESO + FTSMC method in this article has the strongest disturbance rejection ability, smallest speed drop, fastest transient response, smallest chattering, and lowest current ripple among all these control methods under different operating conditions.

B. Experiments and Analysis

In order to verify the feasibility of the proposed control method, an experimental platform has been developed in the laboratory, as shown in Fig. 13. The circuit diagram of the testing platform is given out in Fig. 14. As seen from Figs. 13 and 14, a three-phase rectifier is implemented to provide the dc power. A PWM converter is adopted to drive the PMSM. The sampling

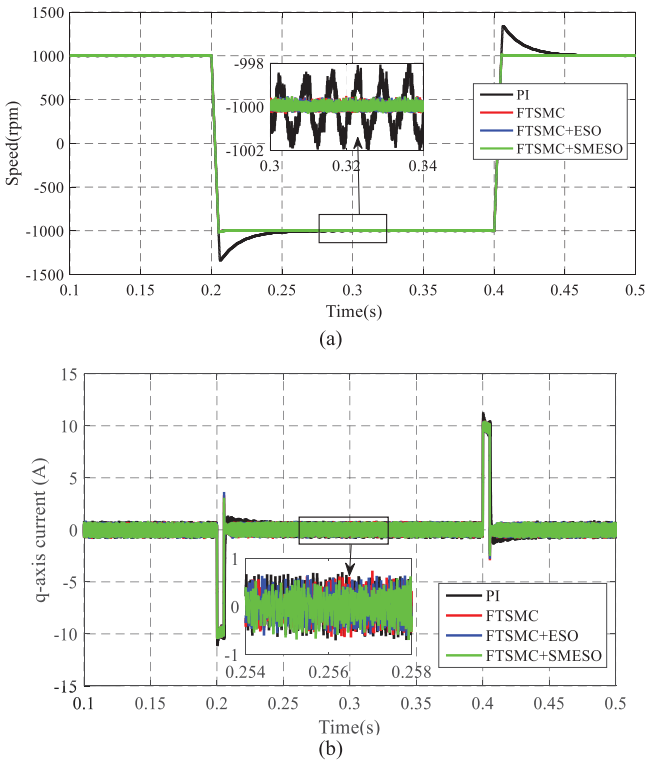

Fig. 12. Reversal and steady-state responses of PI, FTSMC, FTSMC + ESO, and SMESO + FTSMC methods during 1000 to −1000 rpm. (a) Speed. (b) q-axis current.

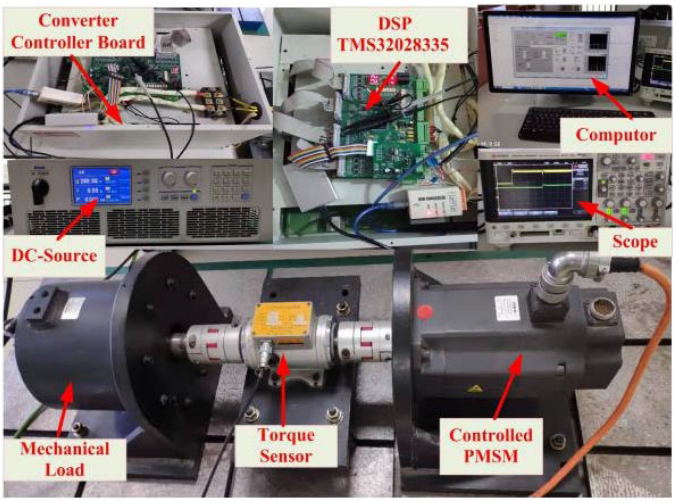

Fig. 13. Photo of the test bench.

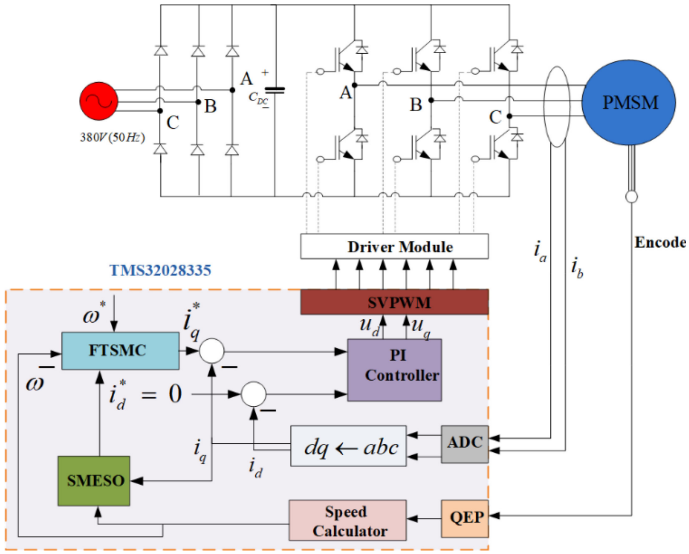

Fig. 14. Circuit diagram of the test platform.

TABLE III
CONTROLLER SPECIFICATIONS ON FOUR CONTROL METHODS

Parameters	Values and Units
PI gains of current controller (with PI)	100 and 50
PI gains of speed controller (with PI)	50 and 20
PI gains of current controller under FTSMC	1 and 1000
Saturation limit	10 A
Sampling frequency	10 kHz
The gains of FTSMC for speed controller	σ_1=4000, σ_2=4000, k_1=0.001, k_2=100000, α_1=0.9, α_2=0.73, and α_3=0.5
The gains of FTSMC+ESO for speed controller	σ_1=4000, σ_2=4000, k_1=0.001, k_2=100000, α_1=0.9, α_2=0.73, α_3=0.5, η_1=200, andη_2=20
The gains of FTSMC+SMESO for speed controller	σ_1=4000, σ_2=4000, k_1=0.001, k_2=100000, α_1=0.9, α_2=0.73, α_3=0.5, η_1=200, and=1000, λ_1=1000, and λ_2=10000

TABLE IV
COMPARISON OF STARTING TRANSIENT PERFORMANCE INDEXES OF THE PI, FTSMC, FTSMC + ESO, AND FTSMC + SMESO METHODS

Control Method	Overshoot (rpm)	Startup Settling Time (s)	Steady State Error(rpm)
PI	160	0.32	± 70
FTSMC	0	0.22	± 56
FTSMC+ESO	50	0.18	± 40
FTSMC+SMESO	0	0.09	± 35

frequencies of both speed and current loops are chosen as 1 and 10 kHz, respectively. The control algorithms have been executed in a DSP controller TMS32028335.

In response to the aforementioned simulations, related experiments have been successfully done and analyzed in details. Main control parameters for the speed and current loops based on the PI, FTSMC, FTSMC + ESO, and SMESO + FTSMC methods are listed in Table III. More details will be given out as follows.

1) Case-1. Starting and Steady-State Performance Under No-Load: The starting speed and q-axis current responses of the PMSM under the control of PI, FTSMC, FTSMC + ESO, and FTSMC + SMESO methods are fully compared, as given out in Fig. 15. As seen from Fig. 15(a), the PI and FTSMC + ESO methods have an overshoot of 160 and 50 rpm, respectively, while the FTSMC and FTSMC + SMESO methods have no overshoot during the starting process under no-load condition.

TABLE V
COMPARISON OF ANTIDISTURBANCE TRANSIENT PERFORMANCE OF THE PI, FTSMC, FTSMC + ESO, AND FTSMC + SMESO METHODS

Control Method	Speed Drop (rpm) and Settling Time (s) with 5 NmLoad		Speed Drop (rpm) and Settling Time (s) at the Load of 10 Nm		Speed drop (rpm) and Settling Time (s) at the Load of 12 Nm	
PI	152	0.150	273	0.33	364	0.41
FTSMC	122	0.085	273	0.22	364	0.43
FTSMC+ESO	88	0.050	235	0.22	272	0.43
FTSMC+SMESO	57	0.020	187	0.17	260	0.07

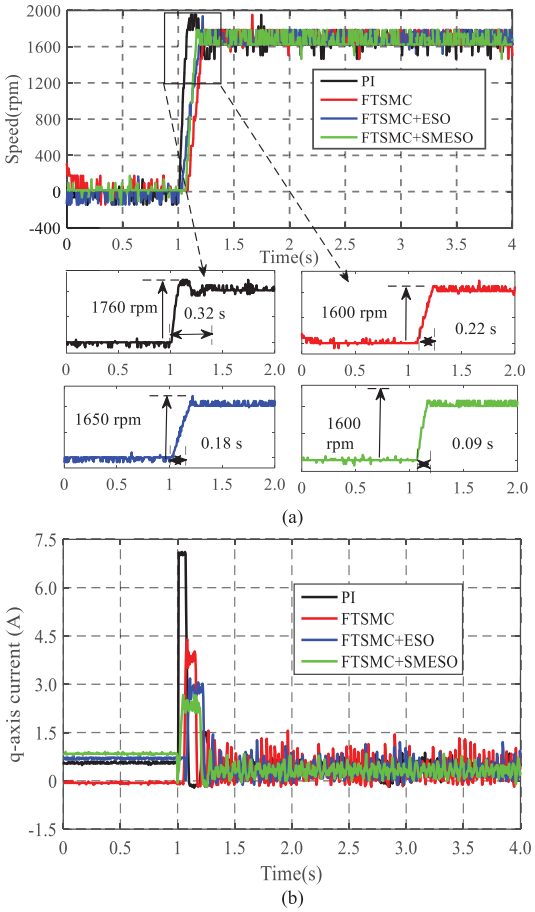

Fig. 15. Startup and steady-state responses of PI, FTSMC, FTSMC + ESO, and FTSMC + SMESO methods under no-load at1600 rpm. (a) Speed. (b) q-axis current.

The settling times of the speed responses based on the PI, FTSMC, FTSMC + ESO, and FTSMC + SMESO methods are 0.32, 0.22, 0.18, and 0.09 s, respectively. Hence, it is known that the FTSMC + SMESO control method has the fastest speed response with the smallest steady-state error during the aforementioned four methods.

2) Case-2. System Responses Under Load Disturbances: The speed and q-axis current responses of the PMSM under the control of PI, FTSMC, FTSMC + ESO, and FTSMC + SMESO methods are tested and compared under various loads of 5, 10, and 12 Nm at 1000, 1600, and 1800 rpm, respectively, as shown in Figs. 16 –18.

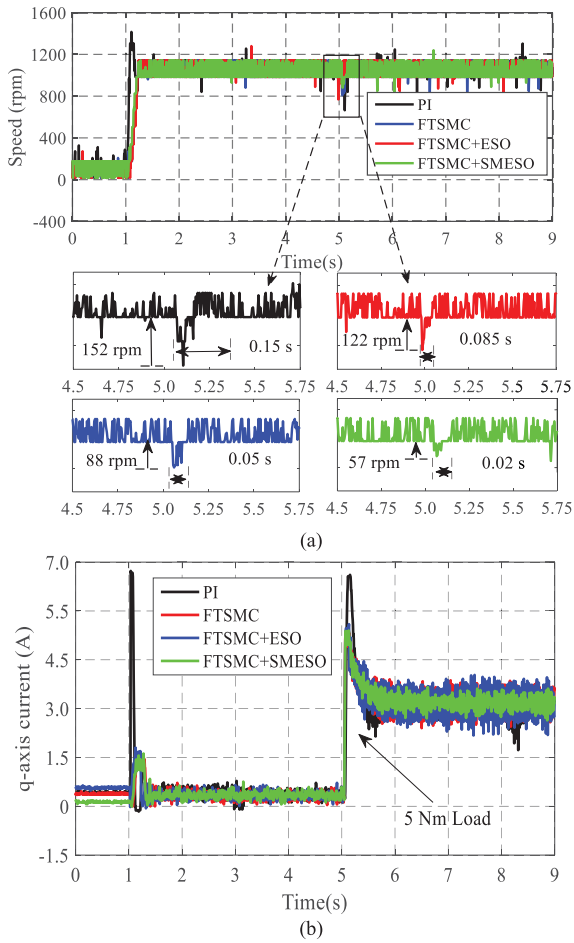

Fig. 16. Sudden load adding responses of PI, FTSMC, FTSMC + ESO, and SMESO + FTSMC methods under the load of 5 Nm at 1000 rpm. (a) Speed. (b) q-axis current.

Fig. 16(a) shows that the settling time of the speed response and the speed drops under the PI, FTSMC, FTSMC + ESO, and FTSMC + SMESO methods with a load of 5 Nm are (0.150 s, 152 rpm), (0.085 s, 122 rpm), (0.050 s, 88 rpm), and (0.020 s, 57 rpm), respectively. As shown in Fig. 16(b), under the FTSMC + SMESO method, the q-axis current response of the PMSM drive system with a load of 5 Nm has the smallest q-axis current ripple and chattering. The conclusion can be drawn from Fig. 16 that the proposed FTSMC + SMESO has quicker speed response under start up and load transient time, which has demonstrated stronger antidisturbance capability than those of PI, FTSMC, and FTSMC + ESO, respectively.

The speed and q-axis current responses of the PMSM under the PI, FTSMC, FTSMC + ESO, and FTSMC + SMESO methods at a load of 10 Nm with reference speed 1600 rpm are shown in Fig. 17. It can be seen from Fig. 17(a) that the settling time of the speed response and the speed drop are (0.33 s, 273 rpm), (0.22 s, 273 rpm), (0.22 s, 235 rpm), and (0.17 s, 287 rpm) under the PI, FTSMC, FTSMC + ESO, and FTSMC + SMESO methods with a load of 10 Nm, respectively. As shown in Fig. 17(b), under the FTSMC + SMESO method, the q-axis current response of the PMSM drive system with a load

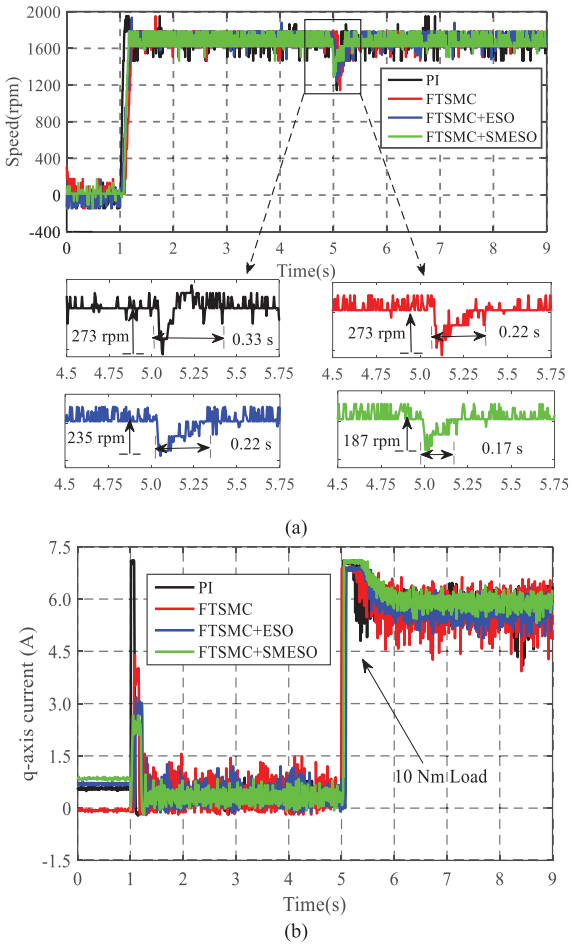

Fig. 17. Sudden load adding responses of PI, FTSMC, FTSMC + ESO, and SMESO + FTSMC methods under the load of 10 Nm at 1600 rpm. (a) Speed. (b) q-axis current.

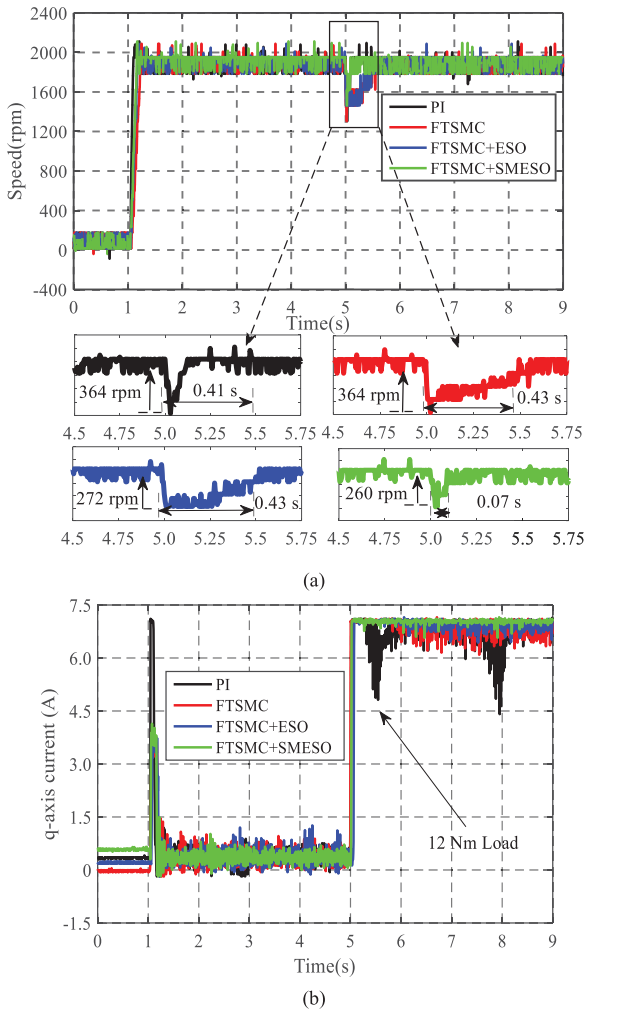

Fig. 18. Sudden load adding responses of PI, FTSMC, FTSMC + ESO, and SMESO + FTSMC methods under the load of 12 Nm at 1800 rpm. (a) Speed. (b) q-axis current.

of 10 Nm has the smallest q-axis current ripple and chattering. Moreover, it can be observed from Fig. 17 that the proposed FTSMC + SMESO has faster speed response under the load transient time and stronger robust antidisturbance ability than those of the PI, FTSMC, and FTSMC + ESO, respectively.

Fig. 18 shows the speed and q-axis current responses under the PI, FTSMC, FTSMC + ESO, and FTSMC + SMESO methods with a load of 12 Nm. As shown in Fig. 18(a), the settling time of the speed response at 1800 rpm under the PI, FTSMC, FTSMC + ESO, and FTSMC + SMESO methods is 0.41, 0.43, 0.43, and 0.075 s, respectively, and the speed drop with a load of 12 Nm is 364, 364, 272, and 260 rpm, respectively. As shown in Fig. 18(b), under the FTSMC + SMESO method, the q-axis current response of the PMSM drive system with a load of 12 Nm has the smallest q-axis current ripple and chattering.

The comparative antidisturbance performance indexes among the PI, FTSMC, FTSMC + ESO, and FTSMC + SMESO are listed in Table VI. As seen from this table, the antidisturbance ability under FTSMC + SMESO has the strongest robust ability at different loads (5, 10, and 12 Nm) and fastest load transient responses among the aforementioned four methods.

VI. Conclusion

In this article, an SMESO is developed to estimate the disturbance in the PMSM drive system, which is implemented with the FTSMC method for the speed control. Main contributions in this article are summarized as follows:

1) One FTSMC method is proposed to ensure the fast convergence, high tracking precision, strong steady-state performance, and small chattering phenomenon effectively.
2) One improved feed-forward compensation method for the speed controller is proposed by combining both SMESO and FTSMC. It can further improve the disturbance rejection ability, reduce the steady-state error of the speed, and minimize the chattering phenomenon effectively.
3) The stability of closed-loop control system combined with SMESO is analyzed by the Lyapunov function.
4) One FTSMC + SMESO method is presented and compared with the PI, FTSMC, and ESO + FTSMC methods against different load disturbances. The superiority of the proposed algorithm is demonstrated persuasively by comprehensive simulation and experiments.

In the next step, the proposed SMESO in this article can be further extended to the current loops for the drive system due to its excellent control performance.

REFERENCES

[1] D. Fodorean, M. Sarrazin, C. Marţiş, J. Anthonis, and H. Auweraer, "Electromagnetic and structural analysis for a surface-mounted PMSM used for light-EV," *IEEE Trans. Ind. Appl.*, vol. 52, no. 4, pp. 2892–2899, Jul./Aug. 2016.

[2] Y. Jiang, W. Xu, C. Mu, J. Zhu, and R. Dian, "An improved third-order generalized integral flux observer for sensorless drive of PMSMs," *IEEE Trans. Ind. Electron.*, vol. 66, no. 12, pp. 9149–9160, Dec. 2019.

[3] L. Harnefors, S. Saarakkala, and M. Hinkkanen, "Speed control of electrical drives using classical control methods," *IEEE Trans. Ind. Appl.*, vol. 49, no. 2, pp. 889–898, Mar./Apr. 2013.

[4] W. Xu, Y. Jiang, C. Mu, and F. Blaabjerg, "Improved nonlinear flux observer based second-order SOIFO for PMSM sensorless control," *IEEE Trans. Power Electron.*, vol. 34, no. 1, pp. 565–579, Jan. 2019.

[5] J. Li, H. Ren, and Y. Zhong, "Robust speed control of induction motor drives using first-order auto-disturbance rejection controllers," *IEEE Trans. Ind. Appl.*, vol. 51, no. 1, pp. 712–720, Jan./Feb. 2015.

[6] B. Wang, C. Lou, Y. Yu, G. Wang, and D. Xu, "Antidisturbance speed control for induction machine drives using high-order fast terminal sliding-mode load torque observer," *IEEE Trans. Power Electron.*, vol. 33, no. 9, pp. 7927–7937, Sep. 2018.

[7] P. Mani, R. Rajan, L. Shanmugam, and Y. H. Joo, "Adaptive fractional fuzzy integral sliding mode control for PMSM model," *IEEE Trans. Fuzzy Syst.*, vol. 27, no. 8, pp. 1674–1686, Aug. 2019.

[8] W. Kim, D. Shin, D. Won, and C. C. Chung, "Disturbance-observer based position tracking controller in the presence of biased sinusoidal disturbance for electrohydraulic actuators," *IEEE Trans. Control Syst. Technol.*, vol. 21, no. 6, pp. 2290–2298, Nov. 2013.

[9] Y. Jiang, W. Xu, C. Mu, and Y. Liu, "Improved deadbeat predictive current control combined sliding mode strategy for PMSM drive system," *IEEE Trans. Veh. Technol.*, vol. 67, no. 1, pp. 251–263, Jan. 2018.

[10] K. Ohnishi, "A new servo method in mechatronics," *Trans. Jpn. Soc. Elect. Eng.*, vol. 107-D, pp. 83–86, Jan. 1987.

[11] Z. Li, C. Su, L. Wang, Z. Chen, and T. Chai, "Nonlinear disturbance observer-based control design for a robotic exoskeleton incorporating fuzzy approximation," *IEEE Trans. Ind. Electron.*, vol. 62, no. 9, pp. 5763–5775, Sep. 2015.

[12] C. Xia, C. Guo, and T. Shi, "A neural-network-identifier and fuzzy-controller-based algorithm for dynamic decoupling control of permanent-magnet spherical motor," *IEEE Trans. Ind. Electron.*, vol. 57, no. 8, pp. 2868–2878, Aug. 2010.

[13] W. Xu, A. K. Junejo, Y. Liu, and M. R. Islam, "Improved continuous fast terminal sliding mode control with extended state observer for speed regulation of PMSM drive system," *IEEE Trans. Veh. Technol.*, vol. 68, no. 11, pp. 10465–104676, Nov. 2019.

[14] S. Li and Z. Liu, "Adaptive speed control for permanent-magnet synchronous motor system with variations of load inertia," *IEEE Trans. Ind. Electron.*, vol. 56, no. 8, pp. 3050–3059, Aug. 2009.

[15] X. Zhang, L. Sun, K. Zhao, L. Sun, and S. Li, "Nonlinear speed control for PMSM system using sliding-mode control and disturbance compensation techniques," *IEEE Trans. Power Electron.*, vol. 28, no. 3, pp. 1358–1365, Mar. 2013.

[16] A. K. Junejo, W. Xu, C. Mu, and Y. Liu, "Improved fast terminal sliding mode control for speed regulation of surface-mounted permanent magnet synchronous motor," in *Proc. Int. Conf. Elect. Mach. Syst.*, Oct. 2018, pp. 93–98.

[17] H. Wang *et al.*, "Continuous fast nonsingular terminal sliding mode control of automotive electronic throttle systems using finite-time exact observer," *IEEE Trans. Ind. Electron.*, vol. 65, no. 9, pp. 7160–7172, Sep. 2018.

[18] E. Kim, "A fuzzy disturbance observer and its application to control," *IEEE Trans. Fuzzy Syst.*, vol. 10, no. 1, pp. 77–85, Feb. 2002.

[19] H. Wang, S. Li, Q. Lan, Z. Zhao, and X. Zhou, "Continuous terminal sliding mode control with extended state observer for PMSM speed regulation system," *Trans. Inst. Meas. Control*, vol. 39, no. 8, pp. 1195–1204, Feb. 2017.

[20] S. S. Xu, C. Chen, and Z. Wu, "Study of nonsingular fast terminal sliding-mode fault-tolerant control," *IEEE Trans. Ind. Electron.*, vol. 62, no. 6, pp. 3906–3913, Jun. 2015.

[21] W. Xu, Y. Jiang, and C. Mu, "Novel composite sliding mode control for PMSM drive system based on disturbance observer," *IEEE Trans. Appl. Supercond.*, vol. 26, no. 7, pp. 1–5, Oct. 2016.

[22] M. Preindl and S. Bolognani, "Model predictive direct speed control with finite control set of PMSM drive systems," *IEEE Trans. Ind. Electron.*, vol. 28, no. 2, pp. 1007–1015, Feb. 2013.

[23] Y. Yi, D. Vilathgamuwa, and M. Rahman, "Implementation of an artificial-neural-network-based real-time adaptive controller for an interior permanent-magnet motor drive," *IEEE Trans. Ind. Appl.*, vol. 1, no. 39, pp. 96–104, Feb. 2003.

[24] M. Reichhartinger and M. Horn, "Application of high order sliding mode concepts to a throttle actuator for gasoline engines," *IEEE Trans. Ind. Electron.*, vol. 56, no. 9, pp. 3322–3329, Sep. 2009.

[25] B. Tian, L. Liu, H. Lu, Z. Zuo, Q. Zong, and Y. Zhang, "Multivariable finite time attitude control for quadrotor UAV: Theory and experimentation," *IEEE Trans. Ind. Electron.*, vol. 65, no. 3, pp. 2567–2577, Mar. 2018.

[26] J. Yang, S. Li, and X. Yu, "Sliding-mode control for systems with mismatched uncertainties via a disturbance observer," *IEEE Trans. Ind. Electron.*, vol. 1, no. 5, pp. 160–169, Jan. 2013.

[27] Y. Feng, X. Yu, and F. Han, "High-order terminal sliding-mode observer for parameter estimation of a permanent-magnet synchronous motor," *IEEE Trans. Ind. Electron.*, vol. 60, no. 10, pp. 4272–4280, May 2013.

[28] R. Dian, W. Xu, J. Zhu, D. Hu, and Y. Liu, "An improved speed sensorless control strategy for linear induction machines based on extended state observer for linear metro drives," *IEEE Trans. Veh. Technol.*, vol. 67, no. 10, pp. 9198–9210, Oct. 2018.

[29] S. S. Xu, C. Chen, and Z. Wu, "Study of nonsingular fast terminal sliding-mode fault-tolerant control," *IEEE Trans. Ind. Electron.*, vol. 62, no. 6, pp. 3906–3913, Jun. 2015.

[30] D. Liang, J. Li, and R. Qu, "Sensorless control of permanent magnet synchronous machine based on second-order sliding-mode observer with online resistance estimation," *IEEE Trans. Ind. Appl.*, vol. 53, no. 4, pp. 3672–3682, Jul./Aug. 2017.

[31] G. Sun, Z. Ma, and J. Yu, "Discrete-time fractional order terminal sliding mode tracking control for linear motor," *IEEE Trans. Ind. Electron.*, vol. 65, no. 4, pp. 3384–3396, Apr. 2018.

[32] A. K. Junejo, W. Xu, C. Mu, M. M. Ismail, and Y. Liu, "Adaptive speed control of PMSM drive system based anew sliding-mode Reaching Law," *IEEE Trans. Power Electron.*, vol. 35, no. 11, pp. 12110–12121, Nov. 2020.

[33] W. Xu, M. M. Ismail, Y. Liu, and M. R. Islam, "Parameter optimization of adaptive flux-weakening strategy for permanent-magnet synchronous motor drives based on Particle Swarm Algorithm," *IEEE Trans. Power Electron.*, vol. 34, no. 12, pp. 12128–12140, Apr. 2019.

[34] G. Sun, L. Wu, Z. Kuang, Z. Ma, and J. Liu, "Practical tracking control of linear motor via fractional-order sliding mode," *Automatica*, vol. 94, pp. 221–235, Aug. 2018.

[35] G. Sun and Z. Ma, "Practical tracking control of linear motor with adaptive fractional order terminal sliding mode control," *IEEE/ASME Trans. Mechatron.*, vol. 22, no. 6, pp. 2643–2653, Dec. 2017.

Wei Xu (Senior Member, IEEE) received the double B.E. and M.E. degrees from Tianjin University, Tianjin, China, in 2002 and 2005, respectively, and the Ph.D. degree from the Institute of Electrical Engineering, Chinese Academy of Sciences, Beijing, China, in 2008, all in electrical engineering.

Between 2008 and 2012, he worked as a Postdoctoral Fellow with University of Technology Sydney, Sydney, NSW, Australia, a Vice Chancellor Research Fellow with Royal Melbourne Institute of Technology, and Japan Science Promotion Society Invitation Fellow with Meiji University. Since 2013, he has been a Full Professor with the State Key Laboratory of Advanced Electromagnetic Engineering, Huazhong University of Science and Technology, Wuhan, China. He has more than 100 papers accepted or published in IEEE Transactions Journals, two edited books published by Springer Press, one monograph published by China Machine Press, and 120 Invention Patents granted or pending, all in the related fields of electrical machines and drives. His research interests include design and control of linear/rotary machines.

Prof. Xu is fellow of the Institute of Engineering and Technology. He has served as an Associate Editor for several journals, such as IEEE TRANSACTIONS ON INDUSTRIAL ELECTRONICS, and so on.

Abdul Khalique Junejo was born in Larkana, Sindh province, Pakistan, in 1989. He received the bachelor's and master's degrees in electrical engineering from Quaid-e-Awam UEST Nawabshah, Sindh, Pakistan, in 2011 and 2015, respectively. He is currently working toward the Ph.D. degree with the School of Electrical and Electronics Engineering, State Key Laboratory of Advanced Electromagnetic Engineering, Huazhong University of Science and Technology, Wuhan, China.

He is currently an Assistant Professor with Quaid-e-Awam UEST Nawabshah, Sindh, Pakistan. His research interests include the sliding mode control, direct torque control, model predictive control and sensorless control methods for permanent magnet synchronous machines, induction machines, and linear IM and drives.

Mr. Junejo has served as a reviewer for the IEEE TRANSACTIONS ON INDUSTRIAL ELECTRONICS, IEEE TRANSACTIONS ON POWER ELECTRONICS, and IEEE TRANSACTIONS ON TRANSPORTATION ELECTRIFICATION.

Yi Liu (Senior Member, IEEE) received the B.E. and M.E. degrees in automation and control engineering from Wuhan University of Science and Technology, Wuhan, China, in 2004 and 2007, respectively, and the Ph.D. degree in mechatronic engineering from Huazhong University of Science and Technology, Wuhan, China, in 2016.

From March to June 2016, he was a Senior R&D Engineer with the Fourth Academy of China Aerospace Science and Industry Group, Wuhan, China. From July 2016 to October 2019, he was a Postdoctoral Research Fellow with the State Key Laboratory of Advanced Electromagnetic Engineering and Technology, Huazhong University of Science and Technology, where he has been a Lecturer since January 2020. His research interests include multiport electrical machines and drive systems.

Dr. Liu is the Vice Chair for the IEEE IES Wuhan Chapter.

Mohamed G. Hussien was born in Zefta, Gharbeya, Egypt, in 1988. He received the B.Sc. and M.Sc. degrees in electrical engineering from the Faculty of Engineering, Department of Electrical Power and Machines Engineering, Tanta University, Tanta, Egypt, in 2011 and 2016, respectively. He is currently working toward the Ph.D. degree with the State Key Laboratory of Advanced Electromagnetic Engineering and Technology, School of Electrical and Electronic Engineering, Huazhong University of Science and Technology, Wuhan, China.

Since 2016, he has been an Assistant Lecturer with the Department of Electrical Power and Machines Engineering, Faculty of Engineering, Tanta University, Tanta, Egypt. His research interests include electrical machines analysis, electrical drives, sensorless control, doubly fed machines, power electronics, and renewable energy systems.

Mr. Hussien has served as a reviewer for IEEE TRANSACTIONS ON INDUSTRIAL ELECTRONICS and IEEE TRANSACTIONS ON POWER ELECTRONICS. His paper has been selected as one of the best papers published in the period (2019–2020) in the IEEE TRANSACTIONS ON ENERGY CONVERSION in the "Power generations systems and grid interfaces" area.

Jianguo Zhu (Senior Member, IEEE) received the B.E. degree from Jiangsu Institute of Technology, Nanjing, China, in 1982, the M.E. degree from Shanghai University of Technology, Shanghai, China, in 1987, and the Ph.D. degree from the University of Technology Sydney (UTS), Sydney, NSW, Australia, in 1995, all in electrical engineering.

In 1994, he was appointed as a Lecturer with the UTS, where he became a Full Professor in 2004 and a Distinguished Professor of electrical engineering in 2017. At UTS, he has held various leadership positions, including the Head of School for School of Electrical, Mechanical, and Mechatronic Systems and Director for Centre of Electrical Machines and Power Electronics. In 2018, he was with the University of Sydney, Sydney, NSW, Australia, as a Full Professor and Head of School of the School of Electrical and Information Engineering. His research interests include computational electromagnetics, measurement and modeling of magnetic properties of materials, electrical machines and drives, power electronics, renewable energy, microgrids, and digital energy systems.